2014-01-01

Analyzing Stress Drops of Earthquakes Near Wellington, New Zealand

Kyle Eugene Barnes
University of Texas at El Paso, kebarnes@miners.utep.edu

ANALYZING STRESS DROPS OF EARTHQUAKES NEAR WELLINGTON, NEW ZEALAND

KYLE EUGENE BARNES

Department of Geological Sciences

APPROVED:

Diane I. Doser, Ph.D., Chair

Aaron A. Velasco, Ph.D.

Sergio D. Cabrera, Ph.D.

Charles Ambler, Ph.D.
Dean of the Graduate School

ANALYZING STRESS DROPS OF EARTHQUAKES NEAR WELLINGTON, NEW ZEALAND

by

KYLE EUGENE BARNES, B.S.

THESIS

Presented to the Faculty of the Graduate School of

The University of Texas at El Paso

in Partial Fulfillment

of the Requirements

for the Degree of

Master of Science

Department of Geological Sciences

THE UNIVERSITY OF TEXAS AT EL PASO

August 2014

Acknowledgements

Thank you for all the guidance and help first and foremost Dr. Doser. I would also like to thank Dr. Rachel Abercrombie of Boston University for her assistance in teaching the basics and giving me the necessary tools with which to accomplish this task. Thanks for answering all of my questions. Thanks also to Carlos Montana with assistance in assembling the coding by which all of this process works. The transfer from Macintosh to Linux was not the smoothest transition. Thanks to the New Zealand GeoNet for all of the waveform data and the seismic moment data.

I would also like to acknowledge all the support I have received from my family that supports me in anything I do, and I would also like to acknowledge my friends and fellow students in their encouragement and support to strive for success.

Abstract

Stress drop studies analyze the change of stress across faults before and after an earthquake. The goal of this study was to determine how stress drop varies throughout the Wellington region of the North Island of New Zealand. To the east of the North Island, the Hikurangi Trough obliquely subducts the Pacific Plate beneath the younger Australian Plate. Toward the southern end of the North Island and into Cook Strait the Pacific plate becomes more buoyant and the plate interface displays strong coupling as subduction diminishes into the strike-slip Marlborough fault system. Subduction of the Pacific plate ceases beneath the South Island and plate motion is taken up along the dextral Alpine Fault. The focus of the study centered on the locked zone of the plate interface extending from Upper Hutt to Cook Strait. Here slow slip events occur downdip of this strongly coupled zone. The study utilizes an empirical Green's function technique to estimate stress drops of earthquake sequences. A deconvolution code removes the path and instrumentation effects. Earthquakes were carefully selected in order to ensure low noise levels and precise estimations of event corner frequencies. Stress drops were calculated based on the corner frequencies and moment magnitudes of the earthquakes chosen. High stress drops were associated with earthquakes within the subducting Pacific plate in the Upper Hutt area. Events occurring in 2004/2005 had an average stress drop of ~1,000 MPa. This was 1-2 orders of magnitude higher stress drops than events occurring in 2006 (~13 MPa) and 2011 (~18.4 MPa) within the same region. The Upper Hutt events were also 1-2 magnitudes higher than the Cook Strait events in 2013-2014. This suggests the slow slip event occurring in 2003 may have more strongly perturbed stresses in the locked zone than a similar event occurring in 2013-2014.

Keywords: New Zealand, stress drop, Cook Strait, empirical Green's function, EGF, Upper Hutt

Table of Contents

List of Tables

List of Figures

Introduction

The island nation of New Zealand features a wide variety of tectonic environments from north to south. The North Island of New Zealand is located above a region where the cold, dense Pacific Plate subducts obliquely underneath the Australian Plate along the Hikurangi Trough at ~39 mm/y (Figure 1). Transitioning towards Wellington, the plate interface becomes strongly locked. Approximately 200 km south of Wellington deep seismicity ceases and oblique plate motion transfers to the strike-slip Marlborough Fault System. This system transfers stresses onto the dextral Alpine Fault along the western South Island. At the southern end of the South Island, a young subduction zone, the Puysegur Trench, features the reverse of the Hikurangi trough with the Australian Plate subducting beneath the Pacific Plate at ~40 mm/y.

The locked zone beneath the southern end of the North Island presents a unique environment and is the focus of this study. Wellington, the capital of New Zealand, and its suburbs, including the suburb of Upper Hutt, are situated on the Australian Plate. This area, along with the Cook Strait that separates the North and South Islands, contains locked portions of the plate interface. The plate interface lies at around 25 km depth below the two cities and into the strait (Reyners and Eberhart-Phillips, 2009). The behavior of the plate interface changes from north to south within the North Island, with slow slip and creep observed north of Wellington in the Hawkes Bay region transitioning into the locking we observe beneath Wellington itself.

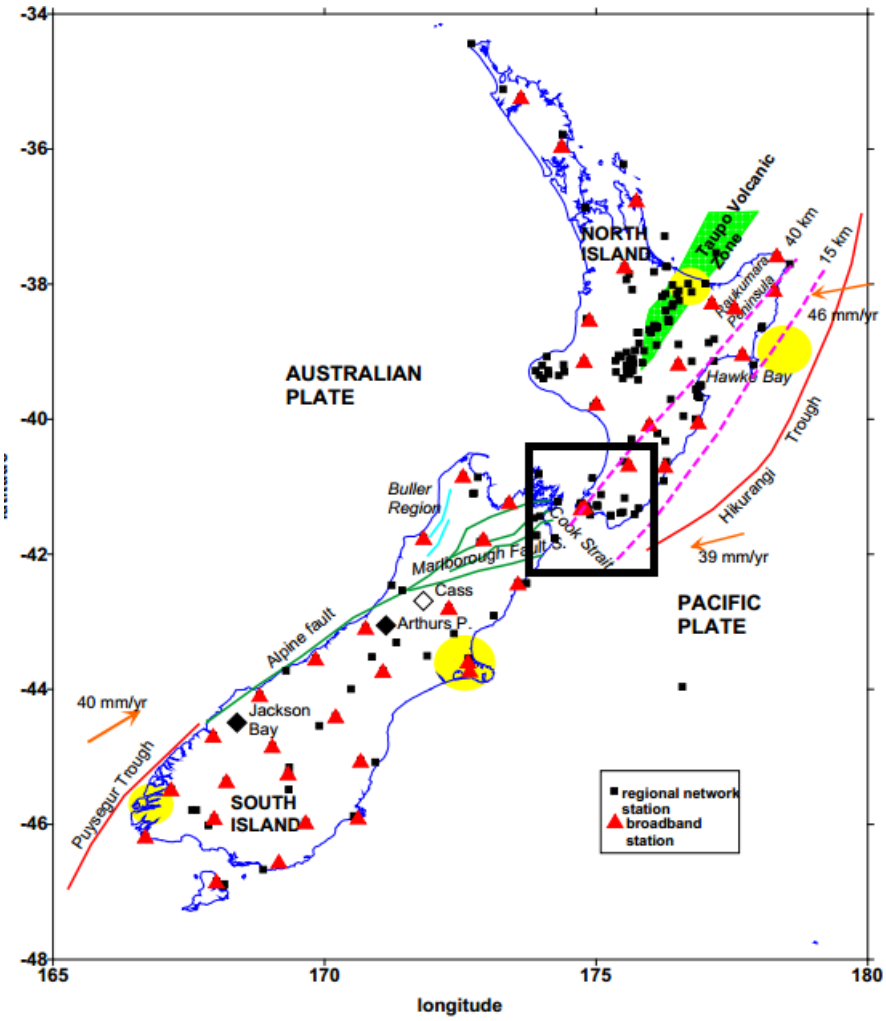

Figure 1. An overview of New Zealand. Notice the oblique subduction of the Pacific Plate under the Australian Plate at the Hikurangi Trough. This is opposite of the subduction on the South Island. The major fault systems are labeled and seismic stations are indicated by red triangles. The black square indicates the area of study.

Historically this region has seen a variety in both earthquake size and locality. Wellington and the Upper Hutt area lie along the Wellington Fault and Wairarapa Fault, both dextral faults in the upper plate, which are among several smaller faults in the area. These crustal faults appear to take up the strike-slip component of plate motion while the plate interface takes up the convergent component of plate motion. These faults extend southwest into Cook Strait where they become part of the Marlborough Fault System. Historical evidence reveals the occurrence of a M~8.2 earthquake in 1855 along the strike-slip Wairarapa Fault located just to the north of Wellington (Sibson, 2006). There also exists paleoseismic evidence for

major events along the Wellington fault. Thus earthquakes of M~7 are reasonable to expect along this fault (van Dissen et al., 1992). No major or great earthquakes (M>~7.0) have occurred along the Wellington or Wairarapa faults since the events in the mid 1800's. Records based on instrumental seismic data for New Zealand only date back into the 1940's and reliable eyewitness reports only reach back to the 1840's. There is some evidence of uplift associated with a major earthquake based on a Maori legend from the 15th Century (Eiby, 1968). However, during the time of modern records, no major plate interface rupture has occurred in the region. Synthetic seismology has been the only way to generate records to predict future events and to reveal past events occurring over 100's to 1000's of years (Robinson et al, 2011). The aseismic activity and slow slip in the region are potential reasons for the lack of interface ruptures in recent history. The buoyant Hikurangi Plateau currently resists subduction producing uplift along the eastern coast of the North Island. This phenomenon occurs in conjunction with the cessation of subduction and the transfer of motion to a strike-slip system. Although events of M~5 have occurred along the plate interface near Cape Palliser in 1990, the potential for larger earthquakes along the plate interface is uncertain (Anderson and Webb, 1994).

The study of stress drops in the Wellington and Cook Strait region around the locked zone will provide insight into how energy transfers through the earth and how stress varies throughout the region. Stress drops measure the effective stress changes in the earth from the time before and after the earthquake occurred. Our measurements of this variable are found using an empirical Green's function (EGF) technique where we utilize a smaller earthquake to remove path and instrument effects from a larger earthquake to infer its source parameters. Through the evaluation of stress drops, we can observe the potential for rapid energy release and how energy relates to the size and depth of the earthquakes within this region. Seismic hazard potential assessments are distinctly intertwined with stress drop and may be influenced based on the results of this study. Higher stress drops lead to more rapidly released energy from the rupture, increasing the likelihood of damage from smaller events.

The New Zealand GeoNet provides good regional instrumental coverage with digital broadband seismographs spaced every ~50 km (Figure 1). While some stations have site effects or noise that limit good signal quality, error measurements account for these and supply more valuable information to the dataset without removing these data. Ultimately this study will be combined with work done collaboratively to assess the variation in stress drop with tectonic regime along both the North and South Islands. An assessment of how effective the EGF technique is in determining stress drop will also be determined as part of the greater study. Numerous earthquakes stress drops, along with the data from this regional study, will demonstrate how the stress drop of a single event compares to several events for a given region. Agreement of the stress drop values is key in establishing the validity of our results and the EGF technique.

1.1 *Geology and Geophysics of Study Area*

The Australian Plate around Upper Hutt is composed of a series of terranes that formed during the Permian and Cretaceous periods. The three main terranes found in the area are the Morrinsville, the Rakaia, and the Pahau Terranes. The Rakaia Terrane is thought to have a low water content or be an impermeable terrane based on its low ratio of P-wave velocity to S-wave velocity (Vp/Vs) compared to the subducting Pacific Plate (Reyners and Eberhart-Phillips, 2009). High P-wave attenuation (Q_p) values in the Pacific Plate in this region indicate a possible high pressure, fluid rich environment.

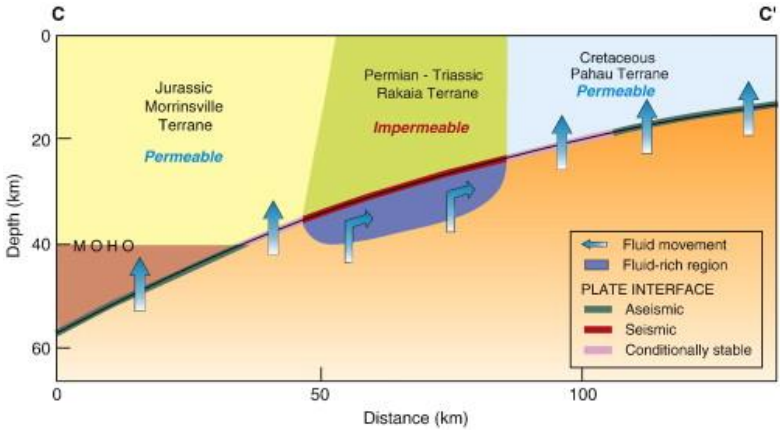

Figure 2. Fluid movement along the plate interface beneath the Rakaia Terrane results in seismic activity along the boundaries of the terranes. (Modified from Reyners and Eberhart, 2009*)*

This contrasts with the Cretaceous Pahau Terrane and Morrinsville Terrane, which have higher Vp/Vs values compared to the underlying Pacific Plate and have higher Qp values than the Rakaia, suggesting that the terranes display permeable or at least less strong material composition. Most seismic activity occurs along the boundary between the Rakaia and the two surrounding terranes and along the plate interface below the Rakaia Terrane. The seismic activity directly relates to the locking interaction of the terrane and the Pacific plate.

A locked zone (the Rakaia) adjacent to stable sliding zones (the Morrinsville and Pahau) provide a theoretically ideal setup for the occurrence of slow-slip events (McCaffrey, et al., 2008). Slow-slip earthquakes (SSE's) occur like regular events but over a period of many days, months, or years, and are caused by fluid flow along the plate interface (Reyners and Eberhart-Phillips, 2009). High pore pressures and low stress zones may be associated with the deep SSE's seen in the North Island (Bartlow, et al., 2014). Rather than a rupture slipping violently and suddenly, a slow-slip event ruptures over a much greater period of time without inducing damaging ground motions. The events are detected through the use of GPS stations established across the island. Since the fluid cannot flow from the subducting plate into the relatively impermeable Rakaia terrane, it must flow laterally along the plate interface to the more permeable terranes. Thus we would expect to see higher stress drop events beneath and near the edges of the Rakaia terrane, where fluid pressures should be high. However, due to the low stress thought to relate to slow slip deeper along the interface, the only way this could happen would be through the excessive loading of stresses on this locked terrain.

Shallow SSE's updip of the creeping and seismic zones have been discovered recently and slow slip may exist all the way up to the trench east of the North Island (Wallace and Eberhart-Phillips, 2013). This feature of dual slow slip zones around the zone of seismic activity demonstrates just how locked the

region is below Wellington. The exceptionally thick Hikurangi Plateau consists of oceanic type crust that is around five times thicker than ordinary crust and contains varying velocity layers that resist subduction and make finding layers like the Moho difficult in some situations (Taylor, 2006).

The slow slip in New Zealand relates to other global examples of subduction zones like the Cascadia subduction zone in the northwest United States and the subduction zone in southern Alaska, as well as zones in Mexico and Japan, where we observe slow-slip earthquake activity. New Zealand is ideally suited for seismicity research with the Hikurangi Trough located only 15 km east of the North Island's shore. No other subduction zone in the world is located this close to land, creating a unique opportunity to better understand seismicity surrounding slow-slip environments. While the locked and creeping zones exhibit differing characteristics, much research remains to understand the impact SSE's have on triggering and stress relations.

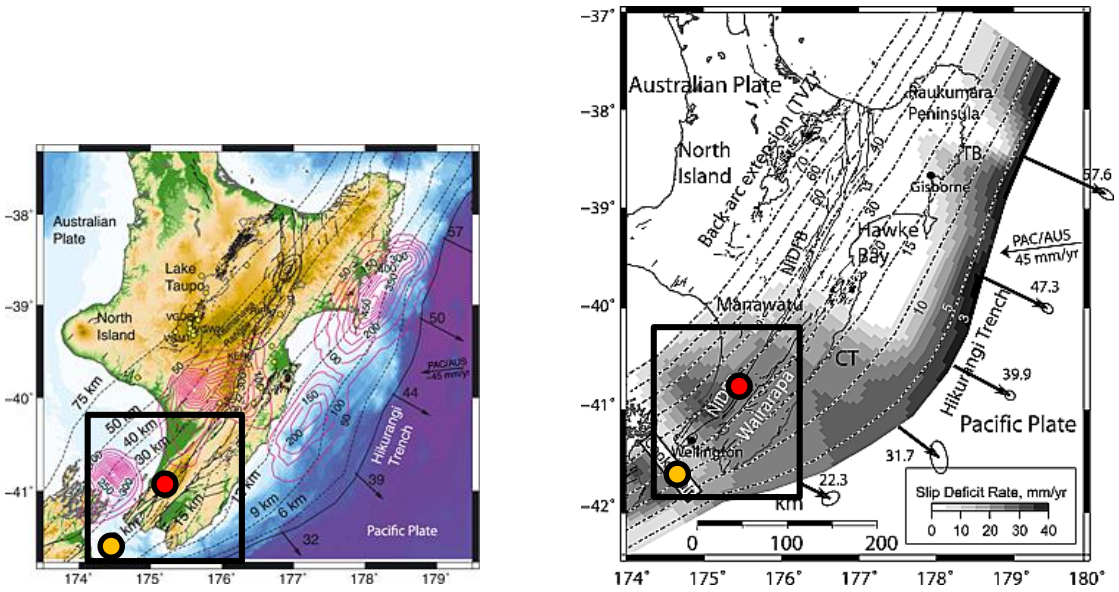

Figure 3. Slow slip events (left) and slip deficit (right) indicating that the region beneath Wellington is locked and that slow slip has various durations and locations. The study area is surrounded by the black box with a notable slow slip event located between the North and South Islands (left). The red circle represents the region of the Upper Hutt clusters while orange is the Cook Strait clusters. The magenta lines denote total observed slip from 2002 to 2012. (Modified from Wallace, 2013 and Wallace and Beaven, 2010)

Slow-slip events have an inherent effect on the stress field in the region. Events occurring downdip

of the locked zone can effectively cause additional loading of the locked zone which in turn could cause high stress drop events or load the locked zone, triggering earthquakes. In the past decade, the Upper Hutt region has experienced several notable seismic swarms, one in April/May 2004 and another in January 2005. These have been analyzed and are documented as events related to slow-slip activity (Figure 3) farther downdip along the plate interface from the swarms' locations (Reyners and Bannister, 2007). Reyners and Bannister (2007) concluded that these two swarms occurred downdip of the locked zone where stable sliding conditions exist causing stress loading updip into the locked zone. Thereby, triggering earthquakes as indicated by the Upper Hutt swarms in the subducted slab at depths of 30 to 40 km. This was part of the first documented slow slip event in the Kapiti region on the east coast of the North Island. Since 2003, researchers have determined that large SSE's occur approximately every five years (2003, 2008, 2013) and release the equivalent of ~M7.0 energy from the crust (Wallace, et al, 2012). The slow slip activity transfers new stresses and relieves others along the faults in the North Island. The 2013 Kapiti Coast SSE began in January 2013 (Figure 4) and potentially altered the stress field enough to trigger the July and August 2013 Cook Strait earthquakes as well as the 2014 Eketahuna earthquake (M~6.2).

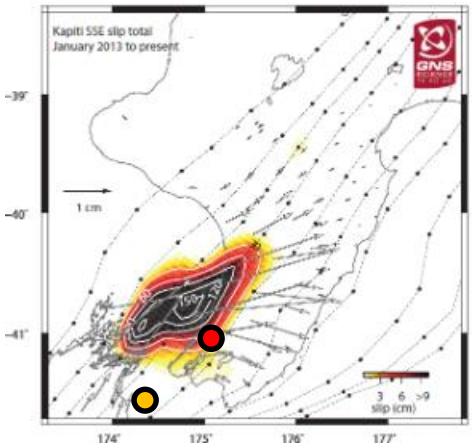

Figure 4. Slip in the Kapiti SSE from January 2013 until early 2014 (still occurring). (Modified from GNS*)*

In the Wellington area, the stick-slip zone below the Rakaia terrane is so strongly coupled that it

creates earthquakes in the subducting slab of the Pacific Plate (Robinson, 2003). These events can then trigger events in the overriding Australian Plate due to the strong coupling across the plate interface. For example, in 1990 two magnitude 6+ earthquakes occurred near the city of Weber. These two events happened only three months apart and were located in the same vertical plane at separate depths, placing the first event in the subducting Pacific plate and the latter event in the upper Australian plate. Robinson (2003) modeled Coulomb failure stress to assess the potential for triggering and established that the first Weber earthquake in February 1990 did likely trigger the second event in May 1990. A similar combination of events occurred in 1942 in the Wairarapa region with the first event in the upper plate and the second in the lower plate (Doser and Webb, 2003). This suggests that due to the locked zone the stress load can be transferred between plates and can trigger future events in the adjacent plate.

Data

The earthquakes considered for this study are associated with the locked zone around the Wellington region and adjacent Cook Strait. The first earthquakes in this study occurred in April/May of 2004 and in January 2005 around Upper Hutt, a suburb of Wellington. The events occurred in the subducting Pacific Plate along normal faults due to unbending of the plate (Figure 5).

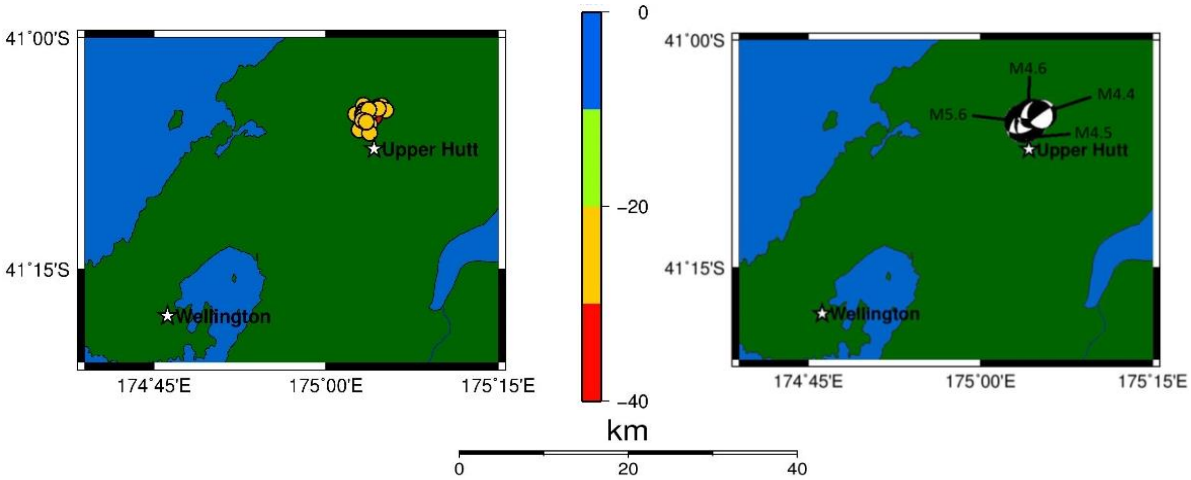

Figure 5. The Upper Hutt swarms occurred around 20-40 km in depth in a highly concentrated area updip of the Kapiti Coast SSE area (left). The earthquakes occurred along normal faults in the subducting Pacific Plate as can be seen by the focal mechanisms for the chosen mainshocks (right).

The Cook Strait sequence occurred during July 2013 and August 2013. Two M~5 events preceded a M~6.5 event in July. In August two M~6 events ruptured a fault in proximity to the July event (Figure 6).

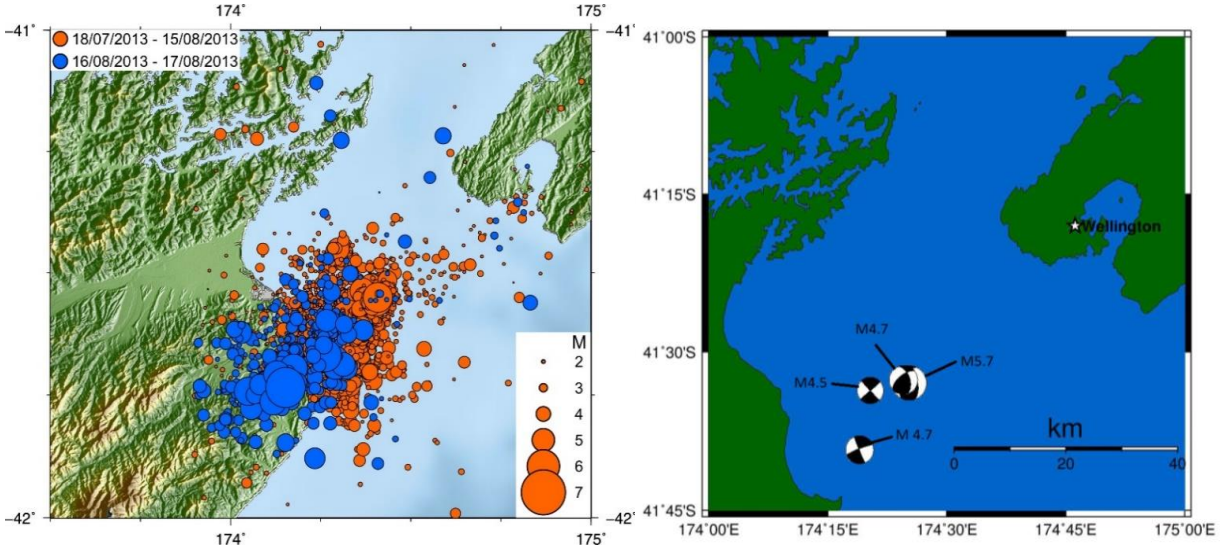

Figure 6. The Cook Strait earthquake sequence occurred in July and August 2013. Orange symbols indicate the mainshock on 21 July 2013 and aftershocks for the July sequence and the blue symbols are the August events associated with the mainshock on 16 August 2013 (left). Focal mechanisms for the four mainshocks used in my research (right). (Modified from GNS)

The data for this research are derived from eight broadband seismographs operated by the New Zealand GeoNet. The GeoNet was modernized to digital instrumentation in 2003. Some of the seismograph stations have only been recording since the early 2000's (NNZ, WAZ, THZ, BKZ) while some have been recording since the early 1990's (BFZ, MRZ, QRZ, TSZ)

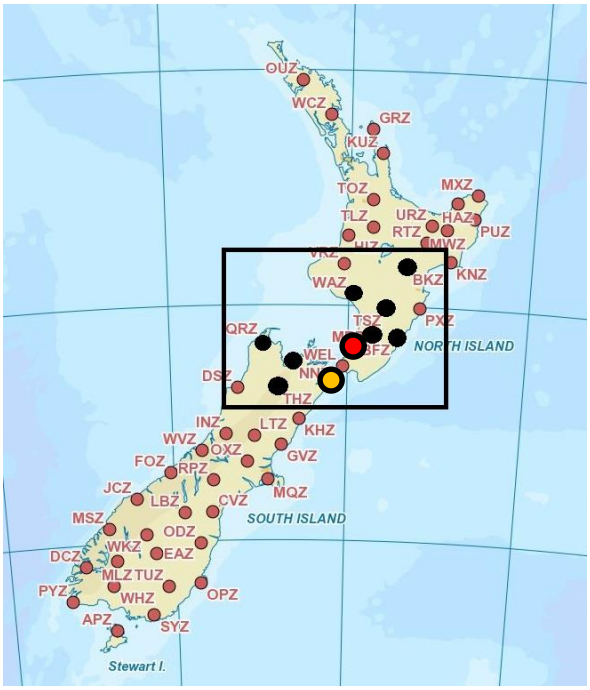

Figure 7. The New Zealand GeoNet. Inset displays stations used for this study (black dots). Red is the region of the Upper Hutt cluster and orange is the Cook Strait cluster (GeoNet, 2014*)*

Since 2003 the network has vastly improved and is very dense with instruments every 50 km. Seismograms and other earthquake information can be downloaded from the Institute of Geological and Nuclear Sciences' (GNS) webpages[1]. All data from the Upper Hutt events and Cook Strait events are

[1] geonet.org.nz

obtained from the eight stations shown in Figure 7. For the Upper Hutt earthquakes, I have used the single magnitude 5 event and three magnitude 4 earthquakes of the sequence in conjunction with several smaller earthquakes to act as empirical Green's functions (EGFs).

For the Cook Strait, a similar choice in mainshocks was conducted using a M~5.7 foreshock to the July events as well as three M~4 events. This allows the two swarms to be compared more readily. As the larger study continues more stations may be incorporated to further determine the validity of the EGF technique and assess the stress drop values.

Methods

This study utilizes the New Zealand GeoNet data and software written in MATLAB and Fortran to analyze waveforms. I perform deconvolutions with an empirical Green's function technique to infer corner frequencies and determine stress drops for the events of the region.

3.1 *Empirical Green's Function*

The empirical Green's Function technique for earthquakes (Hartzell, 1978) employs the use of two earthquakes. The events need to be located < 5-10 km apart and have similar focal mechanisms. For this study I have used criteria that the earthquakes must be < 5 km apart. I use a MATLAB routine to determine which events fit satisfy this criteria. I have also imposed the criterion that the earthquakes' magnitudes should be at least 1 magnitude unit in difference. Smaller magnitude differences may work as well, although the noise relation between source parameters becomes a problem if the difference is too small. These criteria help insure that the smaller event can be considered an impulse response and can be deconvolved from the larger event to effectively remove portions of the waveform signal related to path and instrument effects. A seismogram can be considered as a convolution of several components:

$$x(t) = S(t)*P(t)*I(t) \qquad (1)$$

Where S(t) are the source effects and I(t) are the instrument effects, which are not distance dependent. P(t) represents the path effects, which are distance dependent. If the smaller event is recorded on same instrument, meaning we have the same I(t), and its waves travel the same path, meaning P(t) is the same, then we can deconvolve $X_{EGF}(t)$, the small event seismogram, from $X_{main}(t)$, the large event seismogram to determine $S_{main}(t)$, if we assume $S_{EGF}(t)$ is an impulse response. A conversion from the time domain into the frequency domain is conducted first. Then deconvolution is carried out in the frequency domain to calculate a ratio of the source effects:

$$\frac{F[x(f)main]}{F[x(f)EGF]} = \frac{S(\omega_{main})*G(\omega)*I(\omega)*R(\omega)}{S(\omega_{EGF})*G(\omega)*I(\omega)*R(\omega)} \quad (2)$$

This spectral ratio reduces to:

$$\frac{F[x(f)main]}{F[x(f)EGF]} = \frac{S(\omega_{main})}{S(\omega_{EGF})} \quad (3)$$

The spectral ratio is then used to calculate the corner frequency for the events and eventually the stress drop.

3.2 *Processing*

To process the data, a series of codes have been developed to aid in the cross-correlation and deconvolution of the waveforms following the method of Viegas et al. (2010). (See accompanying flow chart shown in Figure 8)

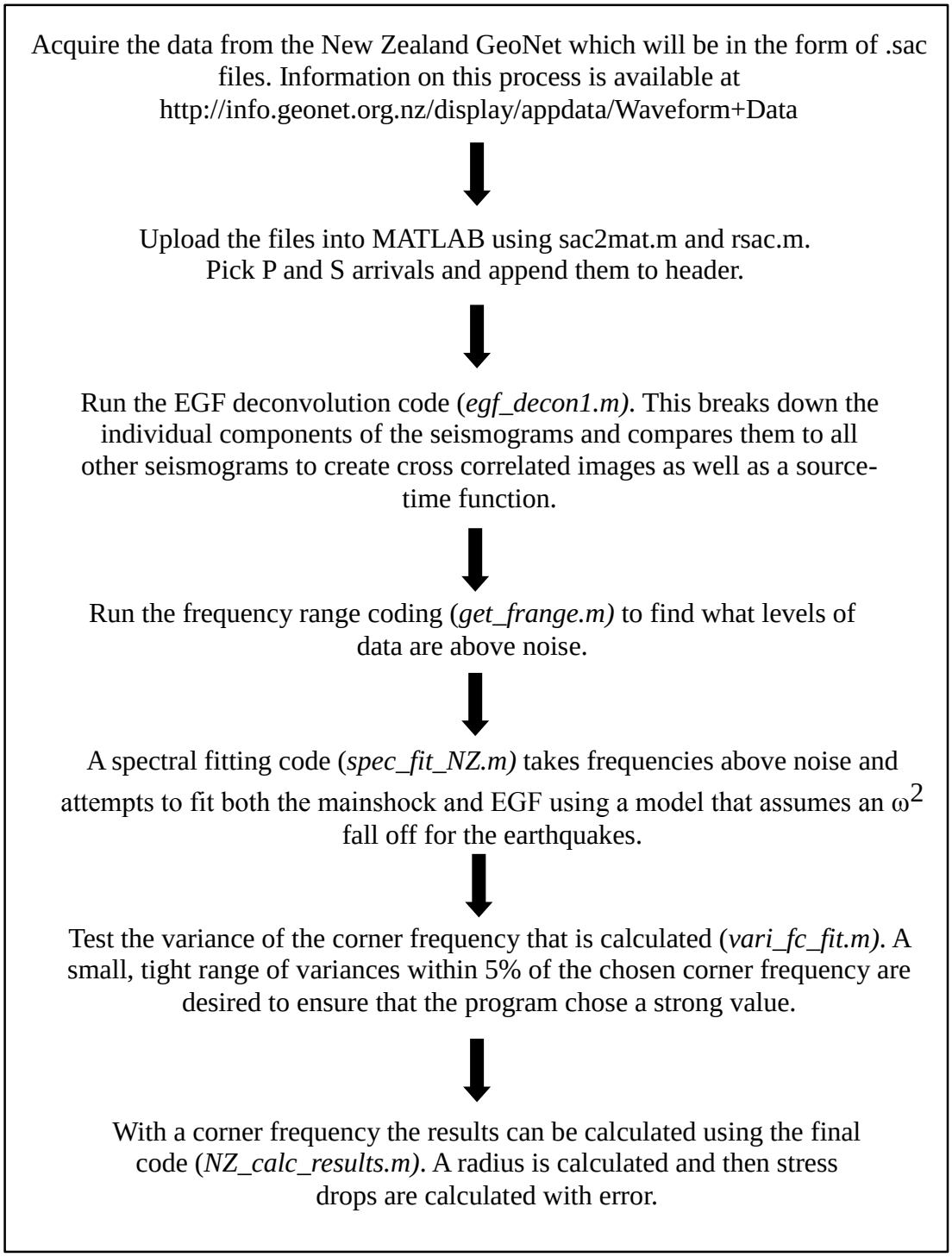

Figure 8. Flow chart for processing.

Egf_decon1.m deconvolves the earthquakes through MATLAB in conjunction with a Fortran based multitaper spectral analysis code developed by Prieto et al. (2009). The waveforms of the larger event and smaller (EGF) event are inspected and cross correlated to ensure a good alignment prior to deconvolution (Figure 9A). The multitaper spectral analysis then produces a spectral ratio following deconvolution (Figure 9B). The spectral ratio is then viewed to determine if both of the earthquakes' corner frequencies are visible. *Egf_decon1.m* also displays the relative source-time function for the spectral ratio which should resemble a single pulse if the EGF cancelled out the path and instrument effects accordingly (Figure 9C). This is due to the fact that I am using the smaller earthquake as a delta function (impulse response) for the larger earthquake. The moment of the larger earthquake can be determined by calculating the area underneath the relative source-time function. For this study I am utilizing moment tensor solution data provided by GNS for calculating the results. The moment relates directly to the stress drop as can be seen in Eq. (5).

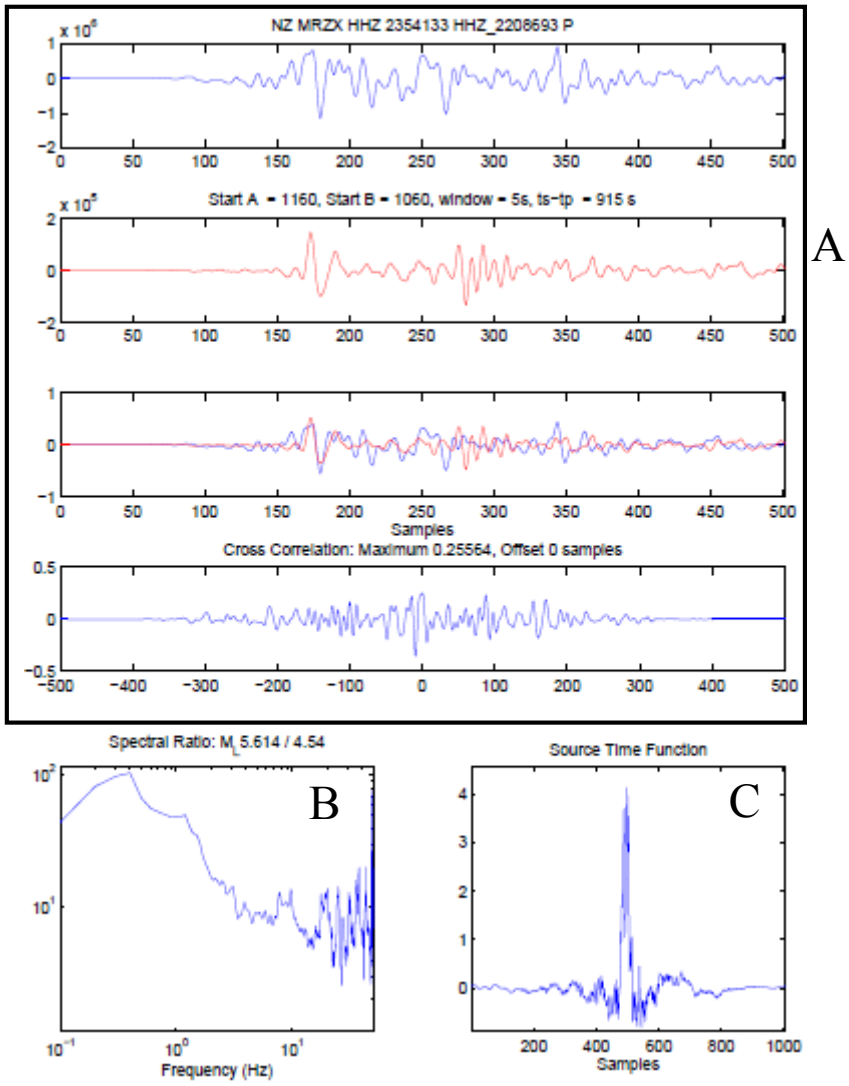

Figure 9. The two earthquakes used in the analysis are shown in (A). The top box represents the larger event (blue) and the second box represents the smaller event (red). The third box here overlays the two events to provide another visual comparison. The fourth box displays the remnant signal after deconvolution. The bottom left box (B) shows the spectral ratio from the deconvolution. The bottom right box (C) contains the source-time function.

Following *egf_decon1.m*, I run *get_frange.m* which finds the frequency range of the correlated waveforms that are above the noise levels (Figure 10B). This allows us to determine how much of the data are worth examining and if reliable corner frequencies can be derived from the given set of frequencies calculated by *egf_decon1.m*. When noise becomes an overwhelming factor these data are less likely to provide ideal results for this study.

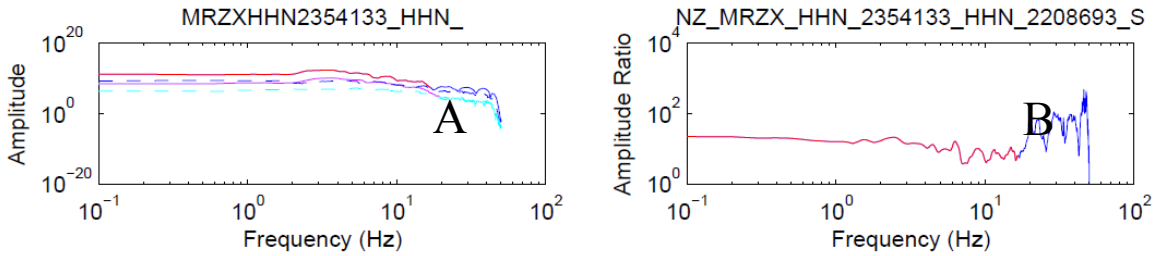

Figure 10. Box A shows a red, a purple, a dashed dark blue, and a dashed light blue line. The red is post P-arrival for the large earthquake and the solid purple line is post-P arrival for the smaller event. Each of the dashed lines represent the pre-P arrival noise, the dark blue is for the large and light blue is for the small event. In Box B, a ratio of the two frequencies is displayed where the red are frequencies 3x above the noise level and the blue are frequencies 3x below the noise level. The latter part of the signal cannot be used to accurately determine a corner frequency.

I then run *spec_fit_NZ.m* to analyze these frequencies and attempt to calculate a corner frequency for both the large earthquake and the small earthquake from the observed spectral ratio. *Spec_fit_NZ.m* attempts to fit an omega squared (ω^2) fall off line to the spectral ratio in order to determine how well the data fit the classic ω^2 model of Brune (1970) (Figure 11).

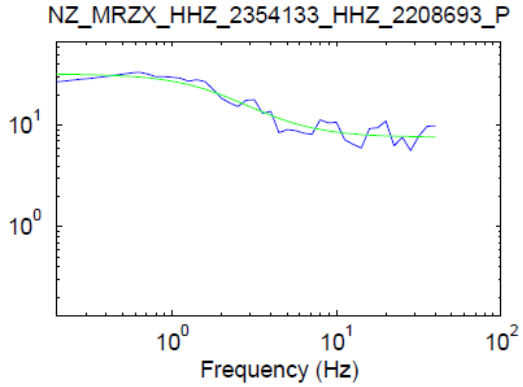

Figure 11. An attempt by the code to fit the theoretical ω^2 fall off line (green line) to the observed spectral ratio (blue line) produced from egf_decon1.m. A wide enough range of frequencies above noise is needed to determine fit. Corner frequencies determined by vari_fc_fit.m are used in conjunction with this fit to determine the best fit to the spectrum.

Brune's model predicts that when a circular fault ruptures it generates seismic waves with frequencies that fall off at a rate ω^2 (Figure 12). I assume the earthquakes in the study represent failure of

circular faults with energy radiating uniformly from the source and that are contained within the crustal limits of the earth. Large earthquakes (> M6.5) cannot be modeled as circular shaped failures due to their immense size and the bound that the crustal thickness places on the width of a fault. Brune's model also predicts that the body waves of larger earthquakes have lower corner frequencies than smaller earthquakes.

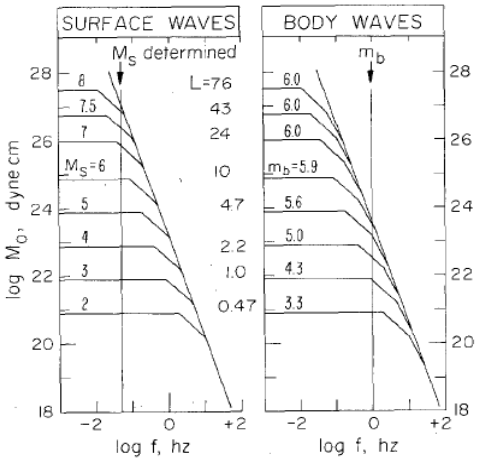

Figure 12. The Brune model for ω^2 fall off shows how corner frequency is greater for smaller earthquakes and saturates for larger events on differing magnitude scales. (Geller, 1976)

Vari_fc_fit.m checks the accuracy and fit of the corner frequency chosen for the large and small event (Figure 13A) by *spec_fit_NZ.m*. This is done by testing a range of possible alternative frequencies to determine if the corner frequency fit is any better than the initial result. Results should show a small range of possible corner frequencies. The slope of the spectral curve below the corner frequency should be close to that of ω^2 (Figure 13B). The corner frequency values should be in a range expected for the seismic moments of the two events (Figure 13C).

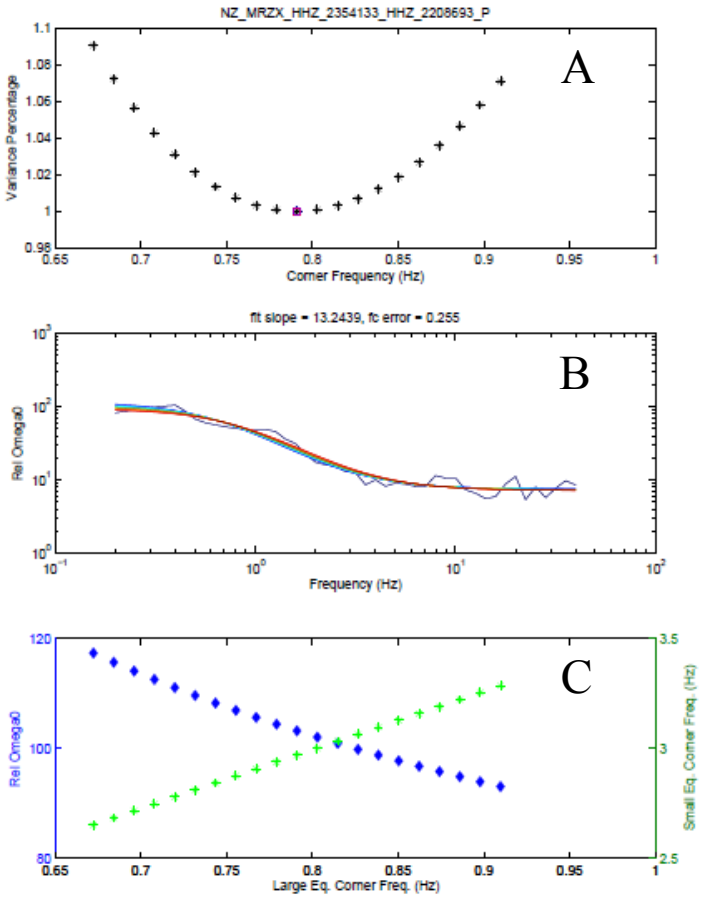

Figure 13. Once an initial corner frequency is estimated, the code attempts to fit several nearby corner frequency values (A) to the observed spectral ratio. A small value spread in corner frequencies (under the 5% threshold) is desirable. In Box B the program attempts to fit several variations of functional corner frequencies (colored smooth lines) to the observations (blue line). A small range of frequencies and a low error % are desirable. Box C shows optimal frequencies for each of the events. The blue diamonds are the best fitting corner frequencies for the large event and the green pluses for the small event. Where the lines intersect is the best fit for both events.

The stress drop ($\Delta\sigma$) can be calculated using a formula that includes the seismic moment (M_0) and the radius of the rupture (r),

$$r = \frac{k\beta}{f_c} \qquad (4)$$

Where k is a constant (0.32 for P-waves and 0.21 for S-waves) and β is the shear velocity (Madariaga, 1976). Corner frequency is particularly important in this equation due to the relation of the radius and the

fact that it is a cubed factor in the static state equation from Eshelby (1957) that I am using to calculate stress drops.

$$\Delta\sigma = \frac{7}{16}\frac{M_0}{r^3} \qquad (5)$$

These calculations are all performed in MATLAB by *NZ_calc_results.m.* The calculations include error estimation through mean values and an inverse variance weighted method.

Results

Within the Wellington Region I have focused on two distinct areas. I have used four individual clusters in the Upper Hutt area in relation to the 2004/2005 swarm and have also used four clusters from the Cook Strait in relation to the July/August 2013 series of earthquakes. These four clusters in Upper Hutt included one M~5.6 event and three M~ 4 events from the locality of the swarms to infer apparent static stress drop while similar clusters were used from the Cook Strait in an interest of comparison of the static stress drops.

The results were calculated using inverse variance weighting (O'Dell, 1998 and Hartung et al., 2008). This process allows me to take data from several seismic stations and combine all the data I have acquired. I do not have to reject data because I weigh less reliable data to lower their effect on the overall total result. Results from stations with clearer waveforms or closer localities garner higher weights and have a larger influence on the total result. With inverse variance weighting the corner frequencies are redetermined by taking the observations obtained through the coding along with their errors and dividing by the inverse factor of the errors.

$$f_w = {\Sigma f_c/\sigma^2}\Big/{\Sigma 1/\sigma^2} \qquad (6)$$

Where f_c is the originally calculated corner frequency in the coding and σ are the original errors. Subsequently the new errors are then calculated by:

$$\sigma_w = \sqrt{{1}\Big/{\Sigma {1}/{\sigma^2}}} \qquad (7)$$

With these newly determined corner frequency values based on inverse weighting, I obtain a stress drop result using all of the data and find an overall stress drop per EGF. After finding the stress drop per EGF, a standard weighted average was applied to find an average for each cluster.

The EGF's selected followed the aforementioned criteria of one magnitude difference and no more than 5 km separation from the mainshock. Thirty seven events were considered as EGF's from the first cluster in the Upper Hutt sequences surrounding a M~5.6 event that occurred in January 2005. I also analyzed a M~4.5 event from July 2004. Thirty four EGF's were considered for this event. The other two events were from January 2006 and March 2011 in the same locality and tested against many of the same EGF's as the first two events. The results of stress drop estimates for these 4 individual events are listed in the Appendix. In Cook Strait, the clusters of earthquakes were not as tightly confined as the Upper Hutt events leading to fewer events to test against. The M~5.7 event was paired with five EGF's while varying amounts of EGF's were compared to the subsequent M~4 clusters which can also be seen in the Appendix.

After compiling the results per EGF in each of the clusters, I took a weighted average of the EGF stress drop values to calculate an overall stress drop for each cluster. These can be seen in Table 1.

Table 1. Average Weighted Stress Drops Per Cluster

Upper Hutt	Cook Strait
M~5.6	M~5.7
1053.4 MPa	17.7 MPa
M~4.5	M~4.7
967.3 MPa	1755.8 MPa
M~4.4	M~4.7
12.9 MPa	43.8 MPa
M~4.6	M~4.5
18.4 MPa	117.1 MPa

The M~5.6 Upper Hutt earthquake exhibited extremely high stress drop results that range from 183 megapascals (MPa) to over 87,000 MPa. While observing stress drops in the range of 100-300 MPa is not unusual, such high numbers (i.e. >1,000 MPa) are unusual based on global compilations of stress

drops (Viegas, et al., 2010). The use of the Madariaga solution for ruptures will produce stress drops 2 to 5 times higher than other techniques. However, this does not account for such high results. A scientific cutoff is often applied in interest that exceeding the stress of a given locality is not a feasible result. In general, the range here demonstrates that although the EGF technique provides reasonable stress drop estimates using some EGFs, there are some estimates that do not appear fit. Reasons for overestimates of the stress drop may stem from poor waveform matching that still passed checks and balances within the coding to produce an extraneous output. Other possibilities relate to the ability to observe higher frequencies with current technology. As the corner frequency rises, there is a connection to the number in the stress drop calculation. This is due to an assumed smaller radius via Eq. (4) and thus a smaller denominator in the stress drop equation. The instruments in New Zealand are modern but may still see the effect of ground attenuation or limited signal reception due to locality near the city of Wellington.

The M~4.54 event from April 2004 displays a stress drop range from 34 MPa to 31,000 MPa. This shows a slightly lower average than the M~5.6 while having occurred a half a year earlier. This may relate to the style of rupture that was seen in conjunction with this event. The M~4.54 rupture was part of a more widespread cluster of events with numerous aftershocks as compare to the M~5.6, where that particular event released the bulk of the energy and few aftershocks followed.

Cluster #3 from Upper Hutt displays a much lower range of stress drops ranging from 4 MPa to 3700 MPa with the general majority between 5 and 30 MPa. The mainshock occurred in 2006 and may indicate that the stress field varies over time in the region. During this time period there was little or no slow slip events occurring in the Kapiti region.

The mainshock in 2011 also shows a considerably lower range of stress drops than Cluster #1 and Cluster #2. Once again, no SSE activity in the area was documented for this time period. Events ranged from 6 MPa to over 1700 MPa and in general between 10 to 30 MPa.

The events in Upper Hutt display a higher than average stress drop when in comparison to other EGF studies (Figure 14). These are compiled from Viegas, et al. (2010) and reflect studies of smaller earthquake sequences in terms of magnitude. My study incorporates much larger earthquakes on average.

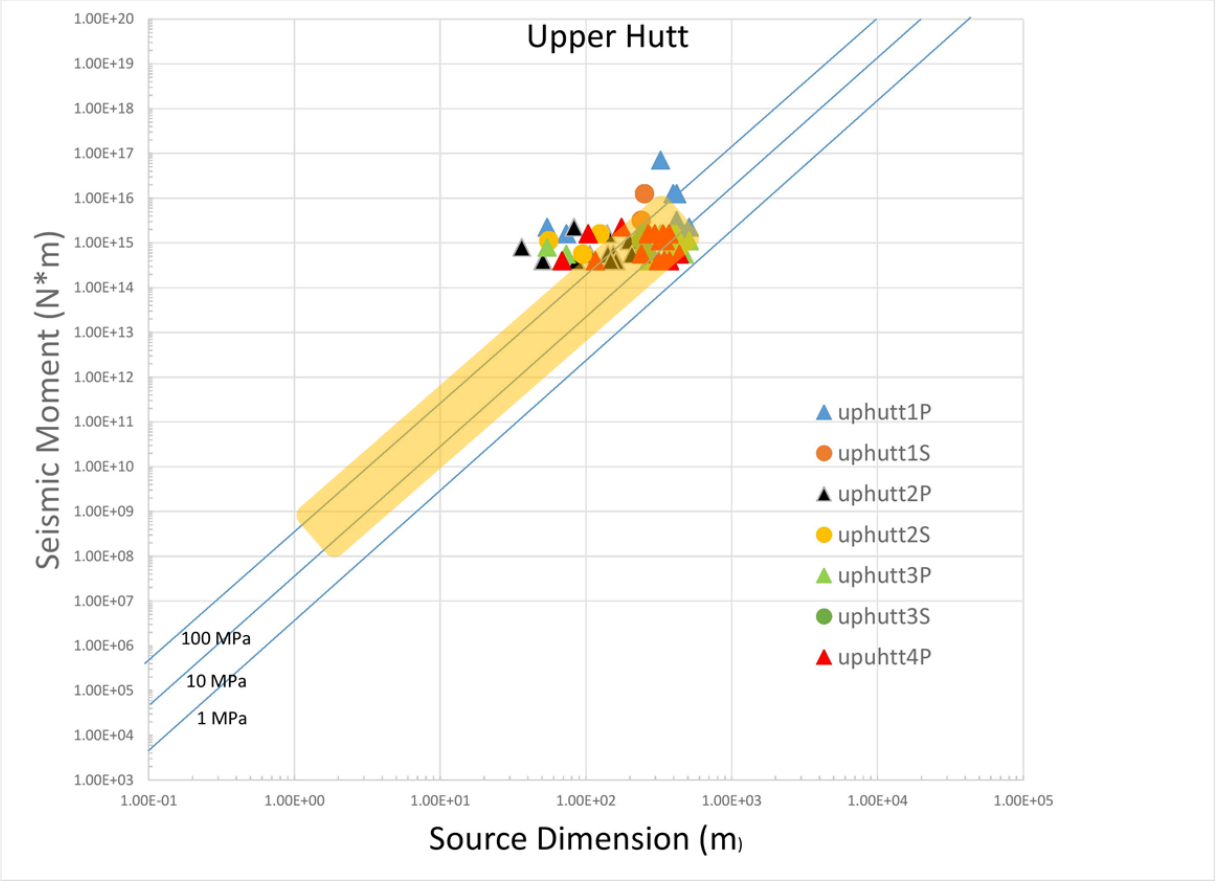

Figure 14. Seismic moments versus source dimension for all the clusters of Upper Hutt. The diagonal lines represent the stress drop. P and S designate the stress drop for each wave and 1, 2, etc. are the clusters. The yellow box displays the range of stress drops calculated by other EGF studies (derived from Viegas, et al., 2010).

The M~5.7 from Cook Strait that I analyzed occurred on 18 July 2013 preceding the larger M~6 earthquake that struck three days later on 21 July 2013. The stress drop values from this smaller grouping range from 11 MPa to 658 MPa. When looking at a direct comparison to the M~5.6 in Upper Hutt, this event does not appear to have nearly as high an average stress drop.

A M~4.7 event occurred on 1 October 2013, a few months after the main events of July/August 2013. From the results in Table 6, only two P waves and three S waves provided corner frequencies. The only tightly constrained value is derived from EGF 2013p542645 where the S wave produced a stress drop of 32 MPa.

This M~4.7 earthquake occurred as an aftershock to the M~6.5, 21 July 2013 event. Several surrounding events allowed a greater set of data to collect better overall results. The general range of stress drops falls between 8 MPa and 80 MPa, while ranging as high as 11,000 MPa.

Cluster #4 from Cook Strait is a transform faulting aftershock on 22 July 2013, this M~4.5 event also had several EGF pairs with the stress drops ranging from 22 MPa to 113 MPa in general with outliers up to 4,000 MPa for P waves. The S waves here are all a magnitude higher and past general acceptance.

These events were also compared in reference to the prior EGF technique studies (Figure 15). Several fall within the high range of previous studies while some exist to the right of the yellow box due to a higher magnitude being used for my study.

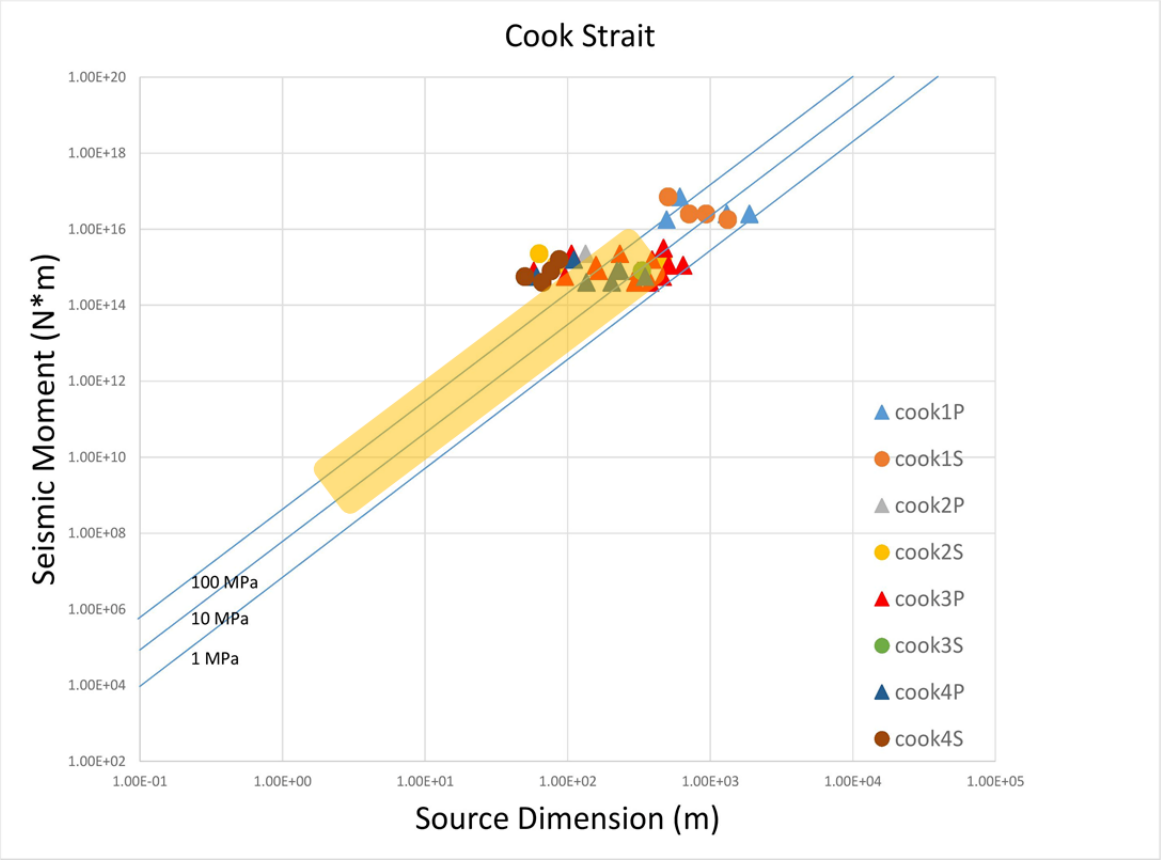

Figure 15. Seismic moment versus source dimension for Cook Strait. Stress drops are diagonal lines across the graph. The yellow box represents the EGF results mentioned in Figure 14 and the triangles and circles represent the clusters and waves of the Cook Strait clusters.

4.1 *Discussion*

While some error has occurred in the calculation of the stress drops, all the data was calculated in the same fashion and thus results can be inferred from the comparison. In Upper Hutt there is a defined gap between the events of 2004/2005 and the subsequent events in 2006 and 2011. A much higher stress drop on average (~1,000 MPa) is found for 2004/2005. This shows that high stress is more than possible in the region and that the slow slip event in 2003 had an impact on the stress in the region. Overall this suggests that the locked zone in the region is indeed inducing high amounts of stress in the surrounding the plate interface. As Figure 3 showed, the slip deficit in Upper Hutt means that despite the lower stress

drop events in 2006 and 2011, a constant loading by SSE's or consistent slip down dip of the locked zone will likely result in another high stress drop event.

When looking in comparison to the Cook Strait stress drops, the events in general do not display the higher stress drops that occurred in Upper Hutt in 2004/2005. The event displaying an average over 1,000 MPa is likely due to lack of data. The amount of slip deficit is also lower in the Cook Strait. The stress drops are similar for the latter two Upper Hutt events and all of the Cook Strait events (10-100 MPa). This suggests that the plate interface beneath the Cook Strait may not be as locked as in the Upper Hutt area and that while larger events did occur in 2013, these are not as threatening as an earthquake near Upper Hutt.

Several factors influenced the results from both Upper Hutt and Cook Strait. The variability and inconsistency related to choosing a corner frequency causes a major conflict. Spectral ratios that appear flat can result from poor cancellation of path or instrument effects. This causes the coding to perceive the "bumps" in the spectra as the corner frequencies (Figure 16). The corner frequency's relation to the radius and subsequently, the stress drop, cubes the error in conjunction with the chosen frequency. This then can alter the results by potentially several magnitudes.

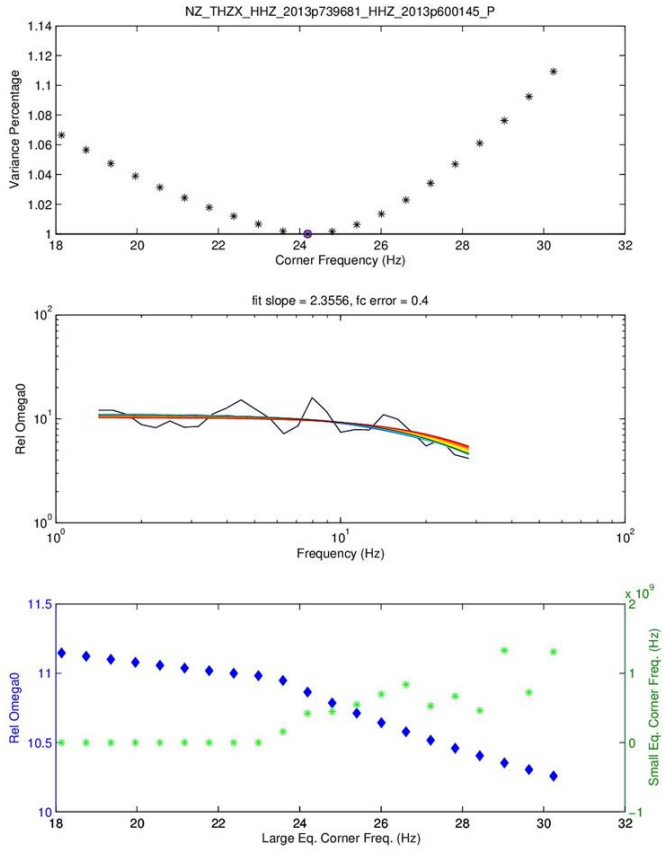

Figure 16. Flat line spectra like the above example can cause poor corner frequency choices. This results in a "bump" in the spectra being called a corner frequency and thus causes invalid stress drop calculations.

Within the coding, a limit to resolve low corner frequencies for larger earthquakes presented a factor that could have altered results. Events like the M~6.5 in July presented difficulty to resolve while the high M~5's were able to be resolved by the coding. Improvements to the coding will be made to correct this issue. With the ability to resolve these large events, I may be able to determine if the largest events in an earthquake sequence produce high stress drop events while the aftershocks remain less threatening.

Poor resolution of waveforms below M~3 limits the number of easily usable EGF's in both areas as well. The Cook Strait events were particularly dispersed making a larger sample size within 5 km harder to obtain. The depth of the Upper Hutt events (20-40 km) influenced the limit of obtaining clear waveforms and differed from the general depth of the Cook Strait sequence (5-20 km).

Focal mechanism plays an inherent role in stress drop calculations as well. In Upper Hutt, normal faulting dominates as seen from the mainshock mechanisms in Figure (5). Some strike-slip events occurred to take up any slip motion however the earthquakes remained similar enough to produce consistent comparisons to remove the path and instrument effects. Leaving comparable source rupture styles to derive a good EGF. Cook Strait contained a variety of differing focal mechanisms. The M~5.7 and one of the M~4.7 are both thrusting events. The majority of the earthquakes in Cook Strait were strike-slip in nature. However, several thrust style earthquakes occurred as the fault ruptured in the Australian Plate. The variation in focal mechanism presents complications for calculating accurate stress drops. A strike-slip does not compare directly to thrusting events. This could be the source of some skewing of my results as far as acceptability. Transform events often are 3-5 times higher than other focal mechanisms (Allmann and Shearer, 2009).

Natural factors in the region including the 5 year cycle of slow slip in the Kapiti Coast along with earthquakes like the Cook Strait in 2013 and the January 2014 Eketahuna sequence influence the major regional stress field. This can alter the stress drop as can be seen from the Upper Hutt clusters. The Cook Strait may have occurred due to variations in the stress field related to the SSE in the Kapiti Coast that began in 2013.

Conclusions

In this study, I took 8 individual clusters of earthquakes from Upper Hutt and Cook Strait near Wellington, New Zealand, and performed an EGF deconvolution technique to infer stress drops. I used strict controls to select quality waveform data to find strong results. I sought to know how the locked zone near Wellington affected stress drop in the region as well as test the EGF technique in a close knit network. I found that the locked zone and slow-slip events both have an influence particularly in the Upper Hutt area and have an effect on the major stresses in the region. These regional effects have led to the occurrence of more than one high stress drop event and will likely lead to another future event in the Upper Hutt area. The EGF technique appears to have a strong consistency and will improve as stronger selection techniques are implemented to refine the errors I have encountered.

References

- Anderson, H., & Webb, T. (1994). New Zealand seismicity: patterns revealed by the upgraded National Seismograph Network. *New Zealand journal of geology and geophysics*, *37*(4), 477-493.
- Bartlow, N. M., Wallace, L. M., Beavan, R. J., Bannister, S., & Segall, P. (2014). Time-dependent modeling of slow slip events and associated seismicity and tremor at the Hikurangi subduction zone, New Zealand. *Journal of Geophysical Research: Solid Earth*, *119*(1), 734-753.
- Brune, J. (1970), Tectonic stress and the spectra of seismic shear waves from earthquakes, *J. Geophys. Res.*, 75, 4997–5009.
- Doser, D. I., & Webb, T. H. (2003). Source parameters of large historical (1917–1961) earthquakes, North Island, New Zealand. *Geophysical journal international*, *152*(3), 795-832.
- Hartung, J., Knapp, G., & Sinha, B. K. (2011). *Statistical meta-analysis with applications* (Vol. 738). John Wiley & Sons.
- Hartzell, S. (1978), Earthquake aftershocks as Green's functions. Geophysical Research Letters, 5: 1–4. doi: 10.1029/GL005i001p00001
- Eiby, G. A. (1968). A descriptive catalogue of New Zealand earthquakes: Part I—Shocks felt before the end of 1845. *New Zealand journal of geology and geophysics*, *11*(1), 16-40.
- Eshelby, J. D. (1957), The determination of the elastic field of an ellipsoidal inclusion and related problems, *Proc. Roy. Soc. Lond., A*, 241, 376–396.
- Madariaga, R. (1976). Dynamics of an expanding circular fault. *Bulletin of the Seismological Society of America*, *66*(3), 639-666.
- McCaffrey, R., Wallace, L. M., & Beavan, J. (2008). Slow slip and frictional transition at low temperature at the Hikurangi subduction zone. *Nature Geoscience*, *1*(5), 316- 320.
- O'Dell, C., & Grayson, C. J. (1998). If only we knew what we know. *California management review*, *40*(3), 154-174.
- Prieto, G. A., Parker, R. L., & Vernon III, F. L. (2009). A Fortran 90 library for multitaper spectrum analysis. *Computers & Geosciences*, *35*(8), 1701-1710.
- Reyners, M., & Eberhart-Phillips, D. (2009). Small earthquakes provide insight into plate coupling and fluid distribution in the Hikurangi subduction zone, New Zealand. *Earth and Planetary Science Letters*, *282*(1), 299-305.
- Reyners, M., and S. Bannister (2007), Earthquakes triggered by slow slip at the plate interface in the Hikurangi subduction zone, New Zealand, Geophys. Res. Lett., 34, L14305, doi:10.1029/2007GL030511.
- Robinson, R. (2003). Fault interactions and subduction tectonics: a re-examination of the Weber, New Zealand, earthquake sequence of 1990.*Geophysical Journal International*, *154*(3), 745-753.
- Robinson, R., Van Dissen, R., & Litchfield, N. (2011). Using synthetic seismicity to evaluate seismic hazard in the Wellington region, New Zealand. *Geophysical Journal International*, *187*(1), 510-528.

- Sibson, R. H. (2006). Charles Lyell and the 1855 Wairarapa, New Zealand Earthquake: Recognition of Fault Rupture Accompanying an Earthquake. *Seismological Research Letters*, *77*(3), 358-363.
- Taylor, B. (2006). The single largest oceanic plateau: Ontong Java–Manihiki–Hikurangi. *Earth and Planetary Science Letters*, *241*(3), 372-380.
- Van Dissen, R. J., Berryman, K. R., Pettinga, J. R., & Hill, N. L. (1992). Paleoseismicity of the Wellington-Hutt Valley Segment of the Wellington Fault, North Island, New Zealand. *New Zealand journal of geology and geophysics*, *35*(2), 165-176.
- Viegas, G., Abercrombie, R. E., & Kim, W. Y. (2010). The 2002 M5 Au Sable Forks, NY, earthquake sequence: Source scaling relationships and energy budget. *Journal of Geophysical Research: Solid Earth (1978–2012)*, *115*(B7).
- Wallace, L. M., & Beavan, J. (2010). Diverse slow slip behavior at the Hikurangi subduction margin, New Zealand. *Journal of Geophysical Research: Solid Earth (1978–2012)*, *115*(B12).
- Wallace, L. M., Beavan, J., Bannister, S., & Williams, C. (2012). Simultaneous long-term and short-term slow slip events at the Hikurangi subduction margin, New Zealand: Implications for processes that control slow slip event occurrence, duration, and migration. *Journal of Geophysical Research: Solid Earth (1978–2012)*, *117*(B11).
- Wallace, L. M., & Eberhart-Phillips, D. (2013). Newly observed, deep slow slip events at the central Hikurangi margin, New Zealand: Implications for downdip variability of slow slip and tremor, and relationship to seismic structure. *Geophysical Research Letters*, *40*(20), 5393-5398.

Appendix

Table 2.1. Upper Hutt Cluster #1 P-Wave						
Seismic Moment = (1.17E+17 N*m)						
publicID	**mag**	**corner P**	**P err**	**radius P**	**stress drop (MPa) P**	**P err**
2354133	5.6					
2208693	4.6	1.80	0.34	623.27	207.80	1.44
2513129	4.5	5.09	1.56	220.24	4709.67	137.26
2354877	4.4					
2227299	4.2	4.89	1.39	228.90	4195.16	97.11
2227285	4	1.83	0.69	612.13	219.35	11.57
3473252	4	2.53	1.08	442.67	578.00	44.52
2552019	3.8					
2208692	3.7					
2215533	3.7	5.46	0.96	204.97	5842.82	31.41
2208721	3.6	4.30	1.00	260.30	2852.54	36.18
3473493	3.5					
2741867	3.5	6.46	0.94	173.26	9673.57	30.09
2441987	3.4					
2208708	3.4	1.86	0.79	602.00	230.62	17.70
2227305	3.4	3.74	0.86	299.18	1878.70	23.13
2552464	3.4	4.21	0.91	266.09	2670.61	27.26
2227688	3.4					
2375159	3.4					
2215550	3.3					
2552934	3.3	3.15	0.65	355.95	1115.64	9.77
2576278	3.3	4.74	1.54	236.04	3825.75	131.33
2752822	3.3					
2354574	3.2					
2576836	3.2	8.41	3.70	133.20	21289.89	1813.56
3351331	3.1	2.89	1.08	387.39	865.41	45.64
3159202	3.1	13.46	5.72	83.18	87421.84	6710.99
2681019	3.1					
2508882	3.1	3.50	1.22	320.08	1534.31	65.78
2450353	3.1					
2356704	3.1	4.32	0.79	259.11	2892.33	17.90
3473308	3	1.72	0.55	650.37	182.89	6.09
2208700	3					
2357646	3	3.36	0.91	333.72	1353.72	26.64
2388389	3	10.15	4.82	110.31	37485.09	4017.34
2358570	3	3.27	0.57	343.01	1246.64	6.68
2305490	3	3.29	0.84	340.63	1272.98	21.48

Table 2.2. Upper Hutt Cluster #1 S-Wave						
Seismic Moment = (1.17E+17 N*m)						
publicID	**mag**	**corner S**	**S err**	**radius S**	**stress drop (MPa) S**	**S err**
2354133	5.6					
2208693	4.6	3.00	0.98	244.64	3436.14	117.96
2513129	4.5					
2354877	4.4					
2227299	4.2	1.63	0.81	451.72	545.83	68.23
2227285	4					
3473252	4	3.63	1.63	202.68	6042.74	550.65
2552019	3.8					
2208692	3.7	1.79	0.85	410.15	729.21	78.15
2215533	3.7					
2208721	3.6					
3473493	3.5	1.09	0.10	676.45	162.54	0.12
2741867	3.5					
2441987	3.4	2.02	0.86	363.34	1048.87	80.52
2208708	3.4					
2227305	3.4	3.85	1.25	190.76	7247.65	248.80
2552464	3.4	3.65	1.03	201.29	6168.54	137.19
2227688	3.4	4.13	1.82	178.11	8904.58	758.53
2375159	3.4	2.80	0.59	262.85	2770.58	25.66
2215550	3.3					
2552934	3.3	2.42	0.69	303.94	1791.83	42.41
2576278	3.3					
2752822	3.3					
2354574	3.2	6.52	2.78	112.66	35184.57	2700.97
2576836	3.2					
3351331	3.1	4.23	1.21	173.72	9597.57	222.18
3159202	3.1					
2681019	3.1					
2508882	3.1	2.73	1.02	269.04	2583.59	136.24
2450353	3.1					
2356704	3.1	3.93	1.12	187.23	7665.12	177.44
3473308	3					
2208700	3	1.24	0.59	590.53	244.32	26.18
2357646	3	7.11	2.67	103.33	45601.98	2404.79
2388389	3					
2358570	3	3.74	0.90	196.50	6631.39	91.67
2305490	3					

Table 2.3. Upper Hutt Cluster #2 P-Wave						
Seismic Moment = (3.49E+15 N*m)						
publicID	**mag**	**corner P**	**P err**	**radius P**	**stress drop (MPa) P**	**P err**
2208693	4.5					
2741867	3.5	13.53	4.06	82.79	2690.72	72.85
2371616	3.5					
2441987	3.5					
2209533	3.5					
2208708	3.4					
2227305	3.4					
2552464	3.4					
3408997	3.4					
2552019	3.4					
2227688	3.4					
2375159	3.4	8.00	2.63	139.95	557.05	19.77
2215550	3.3					
2552934	3.3	3.15	0.87	355.30	34.04	0.71
2576278	3.3	5.67	1.71	197.68	197.66	5.44
2752822	3.3					
2982712	3.2					
2354574	3.2	30.84	14.65	36.31	31893.15	3418.05
2576836	3.2					
3351331	3.1	7.25	1.51	154.41	414.75	3.72
3159202	3.1	10.53	5.06	106.34	1269.79	140.43
2690276	3.1					
2681019	3.1					
2508882	3.1	5.41	2.30	207.02	172.10	13.21
2450353	3.1					
2357842	3.1					
2356704	3.1	7.92	1.30	141.33	540.84	2.39
3473308	3	6.97	2.34	160.64	368.31	13.85
2560704	3	3.26	0.87	343.25	37.75	0.71
2208700	3					
2354468	3					
2357646	3	22.10	3.83	50.67	11734.14	61.18
2388389	3	7.58	1.56	147.73	473.57	4.10
2358570	3	13.08	4.33	85.61	2433.49	88.53
2305490	3	3.95	1.38	283.73	66.85	2.86

Table 2.4. Upper Hutt Cluster #2 S-Wave						
Seismic Moment = (3.49E+15 N*m)						
publicID	**mag**	**corner S**	**S err**	**radius S**	**stress drop (MPa) S**	**S err**
2208693	4.5					
2741867	3.5					
2371616	3.5					
2441987	3.5					
2209533	3.5					
2208708	3.4	5.87	2.20	125.11	779.68	41.12
2227305	3.4					
2552464	3.4					
3408997	3.4					
2552019	3.4					
2227688	3.4					
2375159	3.4					
2215550	3.3					
2552934	3.3					
2576278	3.3					
2752822	3.3	13.18	5.27	55.76	8805.61	563.56
2982712	3.2					
2354574	3.2					
2576836	3.2					
3351331	3.1					
3159202	3.1					
2690276	3.1					
2681019	3.1					
2508882	3.1					
2450353	3.1					
2357842	3.1					
2356704	3.1	7.76	2.52	94.74	1795.52	61.64
3473308	3					
2560704	3					
2208700	3					
2354468	3					
2357646	3					
2388389	3					
2358570	3					
2305490	3					

Table 2.5. Upper Hutt Cluster #3 P-Wave						
Seismic Moment =(1.35E+15 N*m)						
publicID	**mag**	**corner P**	**P err**	**radius P**	**stress drop (MPa) P**	**P err**
2513129	4.4					
2208708	3.4					
2227305	3.4	3.45	0.57	325.02	17.20	0.08
2552464	3.4					
3408997	3.4					
2552019	3.4	2.67	1.27	419.07	8.03	0.86
2227688	3.4	2.827061	1.00	396.17	9.50	0.41
2375159	3.4					
2215550	3.3					
2552934	3.3					
2551489	3.3	2.67	1.14	419.31	8.01	0.61
2752822	3.3	2.19	0.93	510.36	4.44	0.34
2551529	3.2	20.67	5.66	54.19	3711.70	76.38
2354574	3.2					
3159202	3.1	3.02	1.28	371.17	11.55	0.89
2681019	3.1	2.79	0.97	401.29	9.14	0.38
2240028	3.1	15.28	7.33	73.31	1499.01	165.78
2450353	3.1					
2357842	3.1	2.36	1.12	473.66	5.56	0.60
2356704	3.1					
2208700	3					
2354468	3					
2357646	3					
2552012	3					
2388389	3	4.15	1.87	269.56	30.15	2.75
2358570	3					
2305490	3	3.13	1.33	357.68	12.91	0.99

Table 2.6. Upper Hutt Cluster #3 S-Wave						
Seismic Moment =(1.35E+15 N*m)						
publicID	**mag**	**corner S**	**S err**	**radius S**	**stress drop (MPa) S**	**S err**
2513129	4.4					
2208708	3.4					
2227305	3.4					
2552464	3.4					
3408997	3.4					
2552019	3.4					
2227688	3.4	2.91	1.24	252.61	36.64	2.81
2375159	3.4					
2215550	3.3					
2552934	3.3					
2551489	3.3	3.06	1.11	240.33	42.550	2.03
2752822	3.3					
2551529	3.2					
2354574	3.2					
3159202	3.1	2.89	1.38	253.91	36.08	3.87
2681019	3.1					
2240028	3.1					
2450353	3.1					
2357842	3.1					
2356704	3.1					
2208700	3					
2354468	3					
2357646	3					
2552012	3					
2388389	3					
2358570	3					
2305490	3					

Table 2.7. Upper Hutt Cluster #4 P-Wave						
Seismic Moment = (1.29E+15 N*m)						
publicID	mag	corner P	P err	radius P	stress drop (MPa) P	P err
3473252	4.6					
3473493	3.6					
2741867	3.5	6.39	1.49	175.22	104.91	1.33
2371616	3.5					
2441987	3.5					
2552019	3.5					
2209533	3.5					
2208708	3.4	3.01	1.28	371.91	10.97	0.84
2227305	3.4					
2552464	3.4	10.80	3.51	103.70	506.10	17.37
3408997	3.4	3.30	1.00	339.07	14.48	0.40
2227688	3.4	4.18	1.36	267.70	29.42	1.01
2375159	3.4	3.77	1.17	297.14	21.51	0.64
2215550	3.3	3.21	0.53	349.20	13.25	0.06
2552934	3.3	3.45	0.67	324.43	16.53	0.12
2576278	3.3					
2752822	3.2					
2982712	3.2					
2354574	3.2					
2576836	3.1	4.67	1.44	240.04	40.81	1.21
3159202	3.1					
2690276	3.1					
2681019	3.1	2.56	1.22	437.71	6.73	0.72
2508882	3.1					
2450353	3.1					
2357842	3.1					
2356704	3	16.33	4.41	68.59	1748.84	34.42
3473308	3					
2560704	3					
2208700	3	3.24	1.38	345.44	13.69	1.05
2354468	3					
2357646	3					
2388389	3	9.63	3.61	116.27	359.02	18.93
2358570	3	3.57	1.34	314.03	18.22	0.96
2305490	3	2.98	0.71	375.08	10.70	0.15

Table 2.8. Upper Hutt Cluster #4 S-Wave						
Seismic Moment = (1.29E+15 N*m)						
publicID	mag	corner S	S err	radius S	stress drop (MPa) S	S err
3473252	4.6					
3473493	3.6					
2741867	3.5					
2371616	3.5					
2441987	3.5					
2552019	3.5					
2209533	3.5					
2208708	3.4					
2227305	3.4					
2552464	3.4					
3408997	3.4					
2227688	3.4					
2375159	3.4					
2215550	3.3					
2552934	3.3					
2576278	3.3					
2752822	3.2					
2982712	3.2					
2354574	3.2					
2576836	3.1					
3159202	3.1					
2690276	3.1					
2681019	3.1					
2508882	3.1					
2450353	3.1					
2357842	3.1					
2356704	3					
3473308	3					
2560704	3					
2208700	3					
2354468	3					
2357646	3					
2388389	3					
2358570	3					
2305490	3					

Table 3.1. Cook Strait Cluster #1 P-Wave						
Seismic Moment = (1.81E+17 N*m)						
publicID	**mag**	**corner P**	**P err**	**radius P**	**stress drop (MPa) P**	**P err**
2013p537512	5.7					
2013p575071	4.5	1.83	0.73	612.26	345.02	22.08
2013p690484	4.2	0.59	0.11	1885.94	11.81	0.07
2013p572964	4.2	0.86	0.20	1306.98	35.47	0.42
2013p542688	4.2					
2013p565962	4.1	2.27	0.79	493.61	658.41	28.23

Table 3.2. Cook Strait Cluster #1 S-Wave						
Seismic Moment = (1.81E+17 N*m)						
publicID	**mag**	**corner S**	**S err**	**radius S**	**stress drop (MPa) S**	**S err**
2013p537512	5.7					
2013p575071	4.5	1.45	0.16	506.70	608.69	0.75
2013p690484	4.2	1.03	0.18	713.43	218.07	1.16
2013p572964	4.2	0.78	0.37	938.07	95.93	10.28
2013p542688	4.2					
2013p565962	4.1	0.55	0.11	1327.00	33.89	0.24

Table 3.3. Cook Strait Cluster #2 P-Wave						
Seismic Moment = (5.21E+15 N*m**)**						
publicID	**mag**	**corner P**	**P err**	**radius P**	**stress drop (MPa) P**	**P err**
2013p739681	4.7					
2013p537572	3.7					
2013p544181	3.5					
2013p555890	3.5	8.38	1.95	133.71	1370.65	17.22
2013p542465	3.4					
2013p600145	3.3					
2013p539076	3.3	12.66	3.85	88.47	4731.50	133.08

Table 3.4. Cook Strait Cluster #2 S-Wave						
Seismic Moment = (5.21E+15 N*m**)**						
publicID	**mag**	**corner S**	**S err**	**radius S**	**stress drop (MPa) S**	**S err**
2013p739681	4.7					
2013p537572	3.7					
2013p544181	3.5					
2013p555890	3.5	11.64	2.62	63.14	13019.13	148.30
2013p542465	3.4	1.58	0.18	465.76	32.43	0.049
2013p600145	3.3					
2013p539076	3.3	8.90	2.67	82.57	4731.50	133.08

Table 3.5. Cook Strait Cluster #3 P-Wave						
Seismic Moment = (2.19E+15 N*m**)**						
publicID	**mag**	**corner P**	**P err**	**radius P**	**stress drop (MPa) P**	**P err**
2013p544317	4.7					
2013p622568	3.6	2.38	0.89	470.38	21.90	1.15
2013p546235	3.5	10.54	4.48	106.31	1897.30	145.65
2013p896181	3.5	4.82	2.17	232.35	181.72	16.56
2013p543452	3.4	2.87	0.49	390.57	38.26	0.19
2013p670310	3.3	2.19	0.77	511.31	17.05	0.73
2013p614649	3.3	7.10	2.13	157.78	580.35	15.67
2013p057843	3.3	1.73	0.54	646.50	8.44	0.25
2013p550847	3.2	19.40	8.73	57.75	11837	1078.64
2013p742832	3.2	3.60	1.53	311.44	75.46	5.79
2013p548521	3.2	6.79	3.06	164.84	508.87	46.37
2013p630209	3.2					
2013p544493	3.2					
2013p615803	3.1					
2013p545387	3.1	3.27	0.76	342.88	56.55	0.72
2013p753541	3.1	2.41	0.62	463.78	22.85	0.38
2013p544454	3.1	11.70	2.14	95.70	2600.90	15.85
2013p617007	3.1					
2013p791932	3	3.76	1.11	297.49	86.58	2.23
2013p623146	3					
2013p621466	3					
2013p616328	3					
2013p895833	3	2.94	1.10	380.31	41.44	2.19

Table 3.6. Cook Strait Cluster #3 S-Wave						
Seismic Moment = (2.19E+15 N*m**)**						
publicID	**mag**	**corner S**	**S err**	**radius S**	**stress drop (MPa) S**	**S err**
2013p544317	4.7					
2013p622568	3.6					
2013p546235	3.5					
2013p896181	3.5					
2013p543452	3.4					
2013p670310	3.3					
2013p614649	3.3					
2013p057843	3.3					
2013p550847	3.2					
2013p742832	3.2	2.21	0.94	332.64	61.93	4.75
2013p548521	3.2					
2013p630209	3.2					
2013p544493	3.2					
2013p615803	3.1					
2013p545387	3.1					
2013p753541	3.1					
2013p544454	3.1					
2013p617007	3.1					
2013p791932	3					
2013p623146	3					
2013p621466	3					
2013p616328	3					
2013p895833	3					

Table 3.7. Cook Strait Cluster #4 P-Wave						
Seismic Moment = (7.49E+15 N*m**)**						
publicID	**mag**	**corner P**	**P err**	**radius P**	**stress drop (MPa) P**	**P err**
2013p546148	4.5					
2013p542746	3.4					
2013p602050	3.4	10.12	4.55	110.66	707.08	64.43
2013p544379	3.4					
2013p632099	3.2	5.05	2.27	221.78	87.83	8.00
2013p552132	3.2	4.79	0.83	233.84	74.93	0.38
2013p546095	3.2					
2013p543045	3.2					
2013p542750	3.1	18.43	6.45	60.77	4269.92	183.07
2013p548890	3.1					
2013p543630	3.1					
2013p546558	3.1	3.21	1.52	349.18	22.51	2.41
2013p645576	3.1					
2013p544173	3					
2013p544259	3	8.28	1.48	135.19	387.82	2.20
2013p544129	3					
2013p545005	3	5.51	1.31	203.42	113.82	1.55
2013p546517	3					
2013p639057	3					

Table 3.8. Cook Strait Cluster #4 S-Wave						
Seismic Moment = (7.49E+15 N*m**)**						
publicID	**mag**	**corner S**	**S err**	**radius S**	**stress drop (MPa) S**	**S err**
2013p546148	4.5					
2013p542746	3.4					
2013p602050	3.4	8.42	2.32	87.29	1440.63	30.24
2013p544379	3.4					
2013p632099	3.2					
2013p552132	3.2	9.61	4.32	76.49	2140.56	195.06
2013p546095	3.2					
2013p543045	3.2					
2013p542750	3.1					
2013p548890	3.1	14.62	3.73	50.26	7547.60	125.15
2013p543630	3.1					
2013p546558	3.1					
2013p645576	3.1					
2013p544173	3					
2013p544259	3	11.02	3.58	66.68	3231.79	110.94
2013p544129	3					
2013p545005	3					
2013p546517	3					
2013p639057	3					

Vita

Kyle Barnes was born in Brooksville, Florida in 1989, and was the first son to Paul and Kathryn Barnes. He moved to Tennessee in 1994 with his family and graduated from Sullivan East High School in Bluff City, Tennessee, in 2008. He pursued a degree at East Tennessee State University in Johnson City, Tennessee, with an Academic Performance Scholarship and aid from the Tennessee HOPE scholarship program. Kyle achieved a Bachelor's Degree from East Tennessee State University in Physics with a minor in Geology in the spring of 2012. In the fall of 2012 he began a pursuit of a Master of Science in Geophysics at the University of Texas at El Paso under the direction of Dr. Diane I. Doser. During this degree he taught introductory lab courses in Geological Sciences and presented research at the Seismological Society of America Annual Meeting in Anchorage, Alaska. In Spring 2014 Kyle received an offer to work for Schlumberger, a seismic imaging company based in Houston, Texas. He has accepted the offer and post-graduation of his Master of Science degree at the University of El Paso in Summer 2014, he will begin work in October of 2014 for Schlumberger.

Permanent address: 317 Poplar Hill Lane
Bristol, TN 37620

This thesis was typed by Kyle Barnes